Biomechan Model Mechanobiol (2008) 7:191–202
DOI 10.1007/s10237-007-0085-y

ORIGINAL PAPER

Modeling the mechanical consequences of vibratory loading in the vertebral body: microscale effects

D. A. Dickerson · E. A. Sander · E. A. Nauman

Received: 19 May 2006 / Accepted: 4 April 2007 / Published online: 23 May 2007

Abstract Osteoporosis affects nearly 10 million individuals in the United States. Conventional treatments include anti-resorptive drug therapies, but recently, it has been demonstrated that delivering a low magnitude, dynamic stimulus via whole body vibration can have an osteogenic effect without the need for large magnitude strain stimulus. Vibration of the vertebral body induces a range of stimuli that may account for the anabolic response including low magnitude strains, interfacial shear stress due to marrow movement, and blood transport. In order to evaluate the relative importance of these stimuli, we integrated a microstructural model of vertebral cancellous bone with a mixture theory model of the vertebral body. The predicted shear stresses on the surfaces of the trabeculae during vibratory loading are in the range of values considered to be stimulatory and increase with increasing solid volume fraction. Peak volumetric blood flow rates also varied with strain amplitude and frequency, but exhibited little dependence on solid volume fraction. These results suggest that fluid shear stress governs the response of the vertebrae to whole body vibration and that the marrow viscosity is a critical parameter which modulates the shear stress.

Keywords Osteoporosis · Osteopenia · Low bone mass · Spine · Fluid shear stress · Transport · Mixture theory

D. A. Dickerson · E. A. Nauman (✉)
Weldon School of Biomedical Engineering,
Purdue University, West Lafayette, IN 47907, USA
e-mail: enauman@purdue.edu

E. A. Sander · E. A. Nauman
School of Mechanical Engineering,
Weldon School of Biomedical Engineering,
Purdue University, West Lafayette, IN 47907, USA

1 Introduction

Osteoporosis, a disease characterized by the progressive loss of bone mineral density, affects nearly 10 million individuals in the United States (Davidson 2003). The observed decrease in bone mineral density and bone quality compromises the strength of the bone, leaving afflicted individuals at risk for catastrophic osteoporotic fracture at major load bearing sites, including the hip and the spine (2001). Nearly 1.5 million osteoporotic fractures per year are observed in the US, including 700,000 vertebral fractures (Abbott et al. 1996; Davidson 2003). Vertebral fractures lead to a number of functional difficulties, including chronic pain, that drastically decrease the quality of life for afflicted individuals (Abbott et al. 1996). Clinical intervention is often performed to prevent fractures and avoid fracture related morbidity. Conventionally, osteoporosis treatment consists of pharmaceuticals known to abate bone resorption. In addition, it is well known that bone, including osteoporotic bone, will adapt to changes in the mechanical loading environment (Rubin et al. 2001; Routh et al. 2005; Rumancik et al. 2005). The prevailing hypothesis in this regard has been that large strain levels are the key to triggering an anabolic response. As such, in order to increase bone mass, many patients are also prescribed a vigorous aerobic and strength training regimen to complement the anti-resorptive medication (Verschueren et al. 2004). However, in recent years, it has been demonstrated that delivering a low magnitude, dynamic stimulus via whole body vibration can have an osteogenic effect without the need for large magnitude strain stimulus (Rubin et al. 2002a,b). This may be an advantage for patients who are not physically capable of carrying out a rigorous exercise regimen. Experimental studies utilizing vibration to deliver such loading have been successful in a number of animal models (Fritton et al. 1997; Flieger et al. 1998; Judex et al. 2002,

2003; Rubin et al. 2001, 2002a,b). These experiments have led to the implementation of studies in humans using a variety of loading parameters including frequency, amplitude, and duration (Torvinen et al. 2003; Rubin et al. 2004; Verschueren et al. 2004; Ward et al. 2004). Promising results have shown rate-dependent vibratory loading to effectively slow bone loss in the spines of postmenopausal women (Rubin et al. 2004) and promote bone formation in the vertebral bodies of children with low bone density (Ward et al. 2004).

The mechanisms underlying cortical bone remodeling in response to dynamic stimuli have been a topic of considerable attention (Roelofsen et al. 195; Owan et al. 1997; Turner and Pavalko 1998) and numerous modeling studies (Piekarski and Munro 1977; Otter et al. 1990; Weinbaum et al. 1994; Cowin et al. 1995). The role of vibratory loading in cancellous bone has also been examined, albeit to a lesser extent, particularly with regard to modeling the underlying mechanisms for stimulation. Vibratory loading of cancellous bone has the potential to cause physical deformations, marrow movement, blood transport, interstitial fluid flow, and other biophysical phenomena. Due to such complexity, a description of the specific mechanical signals that may be involved in eliciting anabolic responses in cancellous bone has yet to be detailed. In the specific case of the vertebral body, such information is necessary for determining clinically relevant frequencies and amplitudes for stimulation, thereby allowing the eventual development of optimized therapeutic regimens. As a first step toward gaining such insight for the vertebral body, this investigation utilizes a mixture theory model to estimate interfacial shear stress and blood transport levels within the vertebral body in an attempt to determine which parameters are of prime importance for optimal stimulation of bone growth.

2 Theory

In order to describe the mechanical consequences of vibratory loading, a mixture theory approach is adopted and supplemented with the cellular solid model presented in Sander et al. (2003). The vertebral body consists of a cancellous bone core and several fluid components intermixed within the intertrabecular space. Bone marrow is the chief fluid constituent, but blood, lymph, cells, and interstitial fluid are also present in varying amounts. Often, when fluid is considered as a load bearing constituent in mechanical models of bone, the intraosseous fluids are modeled as one component. For the purposes of this investigation, the fluids will be separated into two constituents: the marrow and the blood, as the blood is separated from other fluids by vessel walls. Each of the phases [bone (s), marrow (m), and blood (f)] is viewed as a constituent of the mixture. Below, kinematic, and mixture equations are derived for vertebral body mechanics. More general mixture formulations can be found in the classical works of Atkin and Craine (1976a,b).

In the context of mixture theory, each constituent is considered an individual continuum with continuum-level properties and kinematics. Each constituent has an intrinsic mass M^α and a volume V^α, where $\alpha = \mathrm{s}, \mathrm{m}, \mathrm{f}$ refers to the constituent. The mixture mass and mixture volume are the sum of all constituent values. The solid phase bounds the mixture. Thus, the mixture volume V at any time t is related to the initial volume V_0 by the Jacobian of deformation gradient of the solid phase J (through the relation $V = JV_0$). Any volume loss is restricted to blood flow from the mixture. As a consequence, the volumetric flow rate of blood is simply the derivative of the volume as a function of time. The mass density of the mixture is obtained by dividing the mixture mass $M = \sum_\alpha M^\alpha$ by its volume V. This density is defined by

$$\rho = \frac{M^{\mathrm{s}} + M^{\mathrm{m}} + M^{\mathrm{f}}}{\mathrm{V}} = \rho^{\mathrm{s}} + \rho^{\mathrm{m}} + \rho^{\mathrm{f}}, \tag{1}$$

where ρ^α is the apparent density of the constituent with respect to the mixture volume. The true density of the constituents is $\rho_{\mathrm{T}}^\alpha = M^\alpha / V^\alpha$. The volume fraction ϕ^α occupied by the α-phase is given by $\phi^\alpha = V^\alpha / V$. This indicates a saturation condition in the mixture. Therefore, at all times

$$\sum_\alpha \phi^\alpha = 1 \tag{2}$$

2.1 Geometry and kinematics

At the microscopic level, cancellous bone contains small trabecular struts (Currey 1984; Mosekilde 1988; Keaveny et al. 2001) that connect in a manner that creates a three-dimensional porous structure. In the vertebral body, cancellous bone appears to contain a somewhat regular array of trabecular struts (Fig. 1), and thus has been idealized as a cellular solid consisting of two repeating unit cells: a rectangular unit cell and an offset unit cell (Sander et al. 2003). Each unit cell consists of a single vertical trabecula, modeled as a circular beam of length L_{V} and diameter D_{V}, and two horizontal trabeculae, also idealized as a circular beam with length L_{H} and diameter D_{H} (Fig. 2). In their study, Sander et al. examined the mechanical and fluid flow characteristics of vertebral cancellous bone and studied the effect of aging on these properties. Using the cellular solid model in conjunction with relevant phenomenological relationships, equations of initial solid volume fraction, offset unit cell content fraction, and Poisson's ratio were formulated (Sander et al. 2003).

The model developed by Sander et al. was based on architectural measures obtained by Mosekilde (1988) and calibrated to the experimental results obtained by

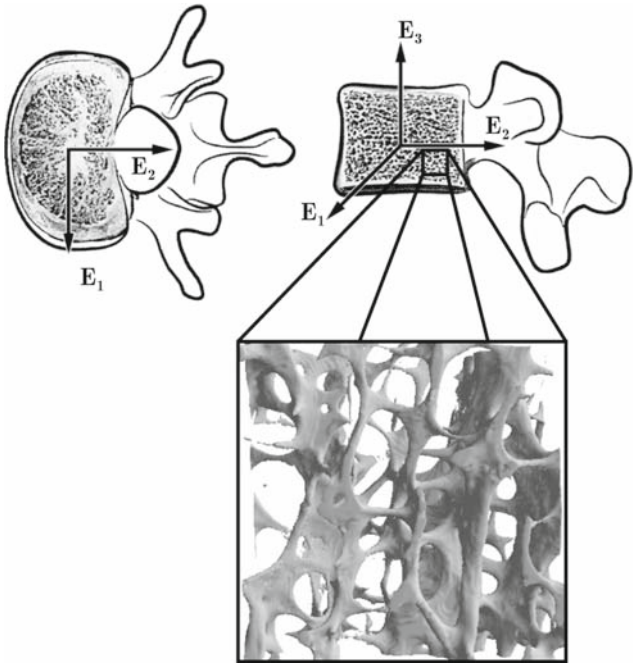

Fig. 1 Transverse and sagittal views of a lumbar vertebrae. The unit vectors, $\mathbf{E_1}$ and $\mathbf{E_2}$ form a basis for the transverse plane while $\mathbf{E_3}$ is oriented in the superior direction. The model assumes that the vibration is directed primarily in the $\mathbf{E_3}$ direction. The *inset* illustrates a three-dimensional rendering of cancellous bone from the human vertebral body (adapted from Sander et al. 2003)

Kopperdahl and Keaveny (1998). While each unit cell geometry possesses a different mechanical response, their initial solid volume fractions (ϕ_0^{s}), were the same:

$$\phi_0^{\mathrm{s}} = \frac{\pi}{4}\left(\frac{D_{\mathrm{V}}^2 L_{\mathrm{V}} + 2D_{\mathrm{H}}^2(L_{\mathrm{H}} - D_{\mathrm{V}})}{L_{\mathrm{H}}^2 L_{\mathrm{V}}}\right). \tag{3}$$

It should also be noted that Sander et al. (2003) assumed a rule of mixtures combination of the two different unit cells. There were two important reasons for this assumption. First, neither unit cell alone could account for the experimentally observed variation in mechanical properties (Morgan and Keaveny 2001; Morgan et al. 2001) when acceptable physiologic values of trabecular tissue modulus were used. The rectangular model was too stiff and the offset rectangular model was too compliant. Second, the rule of mixtures approach provided a useful method for representing the potential load sharing that occurs within the vertebral body. Combining the two models and comparing their mechanical response to the experimentally determined dependence on volume fraction provided an estimate of the changes in structure that occur with aging. This method provides an indication of the fraction of offset unit cells, λ, required to satisfy the model. The parameter, λ, defined as

$$\lambda = \frac{\frac{\pi}{4}\left(\frac{D_{\mathrm{V}}}{L_{\mathrm{H}}}\right)^2 - \frac{b\rho_{\mathrm{T}}^{\mathrm{s}}\phi_0^{\mathrm{s}}}{E_{\mathrm{T}}}}{\frac{\pi}{4}\left(\frac{D_{\mathrm{V}}}{L_{\mathrm{H}}}\right)^2 - \frac{3\pi L_{\mathrm{V}} D_{\mathrm{V}}^2 D_{\mathrm{H}}^4}{12L_{\mathrm{V}}L_{\mathrm{H}}^2 D_{\mathrm{H}}^4 + L_{\mathrm{H}}^5 D_{\mathrm{V}}^2}}} \tag{4}$$

is necessary for relating the microstructure to the apparent level Poisson's ratio, η. The kinematics of the vertebral body are dependent upon, η, given by

$$\eta = \eta_{\mathrm{T}}\left[(1-\lambda)\left(\frac{D_{\mathrm{V}}}{L_{\mathrm{H}}}\right) + \lambda\left(\frac{12L_{\mathrm{V}}D_{\mathrm{V}}D_{\mathrm{H}}^4}{12L_{\mathrm{V}}L_{\mathrm{H}}D_{\mathrm{H}}^4 + D_{\mathrm{V}}^2 L_{\mathrm{H}}^4}\right)\right], \tag{5}$$

where b is a proportionality constant equal to 2.1 GPa cm^3/g (Kopperdahl and Keaveny 1998), E_{T} is the bone's modulus assumed to be independent of anatomic site, age, and geometry, and η_{T} is Poisson's ratio of the solid bone.

Using the preceding definition of Poisson's ratio, and assuming that the macroscopic strain (ε) due to loading in the superior–inferior direction is known, the kinematics of the vertebral body motion can be derived as follows:

$$x_1^{\mathrm{s}} = X_1^{\mathrm{s}} - \varepsilon\eta X_1^{\mathrm{s}}, \tag{6}$$
$$x_2^{\mathrm{s}} = X_2^{\mathrm{s}} - \varepsilon\eta X_2^{\mathrm{s}}, \tag{7}$$
$$x_3^{\mathrm{s}} = X_3^{\mathrm{s}} + \varepsilon X_3^{\mathrm{s}}, \tag{8}$$

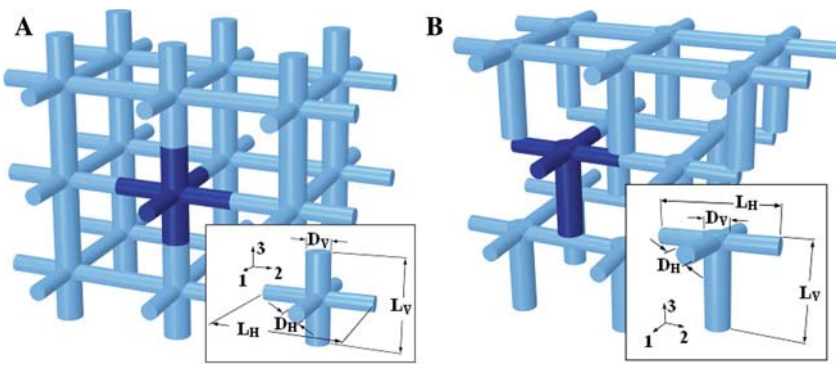

Fig. 2 Cellular solid representation of the cancellous bone in the vertebral body. The mechanical response of the rectangular unit cell **a** and the offset unit cell **b** were combined and calibrated to experimental data to yield relationships for the structural modulus, Poisson's ratio, and permeability (adapted from Sander et al. 2003)

where X_i^{s} describes the reference configuration and x_i^{s} refers to the current configuration. This set of equations results in the following form for the deformation gradient:

$$\mathbf{F}^{\mathrm{s}} = \begin{bmatrix} 1-\varepsilon\eta & 0 & 0 \\ 0 & 1-\varepsilon\eta & 0 \\ 0 & 0 & 1+\varepsilon \end{bmatrix}. \tag{9}$$

As such, the Lagrangian strain tensor of the solid takes the form

$$\mathbf{E}^{\mathrm{s}} = \begin{bmatrix} \frac{1}{2}\varepsilon^2\eta^2 - \varepsilon\eta & 0 & 0 \\ 0 & \frac{1}{2}\varepsilon^2\eta^2 - \varepsilon\eta & 0 \\ 0 & 0 & \frac{1}{2}\varepsilon^2 + \varepsilon \end{bmatrix}. \tag{10}$$

It is assumed that in a vibratory loading regimen, the macroscopic strain of the vertebral body can be expressed in a sinusoidal compression form shown below:

$$\varepsilon = A(\cos\omega t - 1), \tag{11}$$

where A is the amplitude of the vibration at the level of the vertebrae in question, ω is equal to 2π multiplied by the frequency of the stimulus, and t is the time.

2.2 Balance of mass

The general expression for balance of mass of a constituent of a mixture is

$$\frac{\mathrm{D}^\alpha \rho^\alpha}{\mathrm{D}t} + \rho^\alpha \nabla \cdot \mathbf{v}^\alpha = \hat{q}^\alpha \tag{12}$$

where $\mathbf{v}^\alpha$ is the velocity of the α phase, $\hat{q}^\alpha = \rho_T^\alpha \hat{r}^\alpha$ is the rate of mass production per unit volume, and $\frac{\mathrm{D}^\alpha(\hbar)}{\mathrm{D}t}$ is a material time derivative defined as $\frac{\mathrm{D}^\alpha(\hbar)}{\mathrm{D}t} = \frac{\partial(\hbar)}{\partial t} + \frac{\partial(\hbar)}{\partial x_i} v_i^\alpha$. Expanding the previous equation and invoking the incompressibility assumption yields

$$\frac{\partial \phi^\alpha}{\partial t} + \nabla \cdot (\phi^\alpha \mathbf{v}^\alpha) = \hat{r}^\alpha \tag{13}$$

The balance of mass is subject to the constraint

$$\sum_\alpha \hat{r}^\alpha = 0. \tag{14}$$

For simplicity, mass exchanges between the constituents are neglected. The result is the following mass balance equations for mixture constituents:

$$\frac{\partial \phi^\alpha}{\partial t} + \nabla \cdot (\phi^\alpha \mathbf{v}^\alpha) = 0. \tag{15}$$

2.3 Balance of linear momentum

The balance of linear momentum for the mixture constituents can be written as

$$\rho_{\mathrm{T}}^{\mathrm{s}} \phi^{\mathrm{s}} \frac{\mathrm{D}^{\mathrm{s}}\mathbf{v}^{\mathrm{s}}}{\mathrm{D}t} = \nabla \cdot \mathbf{T}^{\mathrm{s}} + \rho^{\mathrm{s}}\mathbf{b}^{\mathrm{s}} + \boldsymbol{\pi}^{\mathrm{s}}, \tag{16}$$

$$\rho_{\mathrm{T}}^{\mathrm{m}} \phi^{\mathrm{m}} \frac{\mathrm{D}^{\mathrm{m}}\mathbf{v}^{\mathrm{m}}}{\mathrm{D}t} = \nabla \cdot \mathbf{T}^{\mathrm{m}} + \rho^{\mathrm{m}}\mathbf{b}^{\mathrm{m}} + \boldsymbol{\pi}^{\mathrm{m}}, \tag{17}$$

$$\rho_{\mathrm{T}}^{\mathrm{f}} \phi^{\mathrm{f}} \frac{\mathrm{D}^{\mathrm{f}}\mathbf{v}^{\mathrm{f}}}{\mathrm{D}t} = \nabla \cdot \mathbf{T}^{\mathrm{f}} + \rho^{\mathrm{f}}\mathbf{b}^{\mathrm{f}} + \boldsymbol{\pi}^{\mathrm{f}}, \tag{18}$$

where $\mathbf{b}^\alpha$ is the body force per unit mass acting on constituent α and $\boldsymbol{\pi}^\alpha$ is an interaction force that accounts for momentum transfer to constituent α from the other constituents. Body forces acting on the constituents are ignored. While typically neglected in mixture theory applications, inertial terms are included in this model due to the dynamic nature of the vibratory loading on the vertebral body. It is assumed that the interaction forces can be described using a Darcy type relation,

$$\boldsymbol{\pi}^{\mathrm{s}} = \mu_{\mathrm{m}} \mathbf{K}_{\mathrm{sm}}^{-1} (\mathbf{v}^{\mathrm{m}} - \mathbf{v}^{\mathrm{s}}) \tag{19}$$

$$\boldsymbol{\pi}^{\mathrm{m}} = -\mu_{\mathrm{m}} \mathbf{K}_{\mathrm{sm}}^{-1} (\mathbf{v}^{\mathrm{m}} - \mathbf{v}^{\mathrm{s}}) + \boldsymbol{\xi} \tag{20}$$

$$\boldsymbol{\pi}^{\mathrm{f}} = -\boldsymbol{\xi} \tag{21}$$

the variable $\boldsymbol{\xi}$ accounting for the interaction between the marrow and the blood is unknown. No interaction term is needed for the blood and the solid as marrow separates the blood vessels from contact with the solid skeleton. The components of the permeability tensor for the marrow are obtained from Sander's derivation (Sander et al. 2003). It is assumed that the viscous behavior of the marrow and the blood can be modeled via interactions between the constituents. The result is the following equation for the velocity of the bone marrow:

$$\mathbf{v}^{\mathrm{m}} = \mathbf{v}^{\mathrm{s}} + \frac{\rho_T^{\mathrm{s}} \phi^{\mathrm{s}}}{\mu_m} \mathbf{K}_{\mathrm{sm}} \frac{\mathrm{D}^{\mathrm{s}}\mathbf{v}^{\mathrm{s}}}{\mathrm{D}t} \tag{22}$$

2.4 Marrow–bone interaction

To develop a better understanding of the mechanical microenvironment on the surface of the trabeculae, we utilize an approach based on the drag theory of permeability to determine the order of magnitude of the shear stress experienced due to marrow movement at the marrow–solid interface. To begin, the microscopic level velocity field was determined by utilizing solutions for flow along the length of a cylinder and around transversely oriented cylinders (Drummond and Tahir 1984). When averaged over a unit cell, these velocities are equivalent to the macroscopic continuum velocity of the marrow as determined by the mixture theory equations.

For flow longitudinal to a cylinder with center-to-center distance l, radius a, and coordinate direction i, assuming a no-slip condition on the surface of the cylinder, the velocity profile in cylindrical polar coordinates is estimated as

$$w_i = \frac{1}{2\mu_m}\frac{\partial p}{\partial x_i}\left[\frac{1}{2}(a^2 - r^2) + \frac{l^2}{\pi}\left\{\ln\left(\frac{r}{a}\right) + \sum_{n=1}^{\infty}\left[\frac{P_{4n}}{4n} - \frac{(4n+3)!}{4!(4n)!}P_4 P_{4n+4}(a/l)^8 + \cdots\right] \times \left(\frac{a}{l}\right)^{4n}\left[\left(\frac{a}{r}\right)^{4n} - \left(\frac{r}{a}\right)^{4n}\right]\cos 4n\theta\right\}\right] \quad (23)$$

P_n is a geometric variable that account for the pattern and spacing of the repeating array of cylinders (Drummond 1984, p. 31). Values for this series are given by

$$P_n = \sum\sum_{p,q\neq 0,0} (p + \mathrm{i}q)^{-n} \quad (24)$$

Using the continuum level velocity derived previously, the drag force acting per unit length of the cylinder is calculated as

$$F_{\mathrm{i}}^{\mathrm{L}}(a, l) = \frac{4\pi\mu v_i^{\mathrm{m}}}{\ln\left(\frac{l^2}{\pi a^2}\right) - 1.476335966 + \frac{2\pi a^2}{l^2} + \frac{1}{2}\left(\frac{\pi a^2}{l^2}\right)^2 - \frac{0.0509713(\pi a^2/l^2)^4}{[1+1.51978(\pi a^2/l^2)^4]}} \quad (25)$$

Similarly, the transverse component of the drag force due to marrow movement is given by

$$F_i^{\mathrm{T}}(a, l) = \frac{4\pi\mu v_i^{\mathrm{m}}}{\ln\left(\frac{l}{a}\right) - 1.310532927 + \frac{\pi a^2}{l^2} - 8.75573387\left(\frac{a}{l}\right)^4 + 63.21721610\left(\frac{a}{l}\right)^6 - 235.8407557\left(\frac{a}{l}\right)^8} \quad (26)$$

To account for the flow at the intersection of the horizontal and vertical struts, an additional component of the drag force was formulated utilizing the procedures previously outlined (Fourie 2002, p. 35; Sander et al. 2003, p. 24). By modeling Poiseuille flow through a pore with a cross sectional area equivalent to that of the unit cell, this component of the drag can be calculated as follows:

$$F_i^{\mathrm{D}}(h, \delta, A_C, A_w) = \frac{128 A_c A_w h \mu v_i^{\mathrm{m}}}{\pi\delta^4} \quad (27)$$

Where δ is the hydraulic diameter, equating the cross sectional area of the unit cell to that of a pore. This term effectively accounts for the increased drag caused by trabecular struts intersecting at right angles and disrupting the idealized flow field predicted by Eqs. (23) and (24).

To complete the solution for the microscale velocity profiles along the length of and transverse to the idealized trabeculae, the pressure drop due to flow was calculated by adding the forces acting on the unit cell and utilizing Darcy's law assumption:

$$\frac{\partial p}{\partial x_1} = \frac{F_{\mathrm{L}}(D_h/2, L_v) + F_{\mathrm{T}}(D_h/2, L_v) + F_{\mathrm{T}}(D_v/2, L_h) + F_{\mathrm{D}}(L_h, D_{eq}, L_h{\bullet}L_v, A_w)}{L_v L_h} \quad (28)$$

$$\frac{\partial p}{\partial x_2} = \frac{F_L(D_h/2, L_v) + F_{\mathrm{T}}(D_h/2, L_v) + F_{\mathrm{T}}(D_v/2, L_h) + F_{\mathrm{D}}(L_h, D_{eq}, L_h{\bullet}L_v, A_w)}{L_v L_h} \quad (29)$$

$$\frac{\partial p}{\partial x_3} = \frac{F_{\mathrm{L}}(D_v/2, L_h) + F_{\mathrm{T}}(D_h/2, L_v) + F_T(D_h/2, L_v) + F_{\mathrm{D}}(L_v, L_h, L_h^2, A_w)}{L_h^2} \quad (30)$$

where

$$A_w = \pi[D_v(L_v - D_h) + 2D_h(L_h - D_v)] \quad (31)$$

and D_{eq} is the diameter of a circular pore with an area and perimeter equivalent to that formed by the unit cell. The shear stress acting on the surface of the cylinders in the longitudinal direction is then calculated using Newton's formula:

$$\tau_i^L = \mu_m \frac{\partial w_i}{\mathrm{d}x_i} \quad (32)$$

The general solution for velocity potential around cylinders oriented transverse to the direction of flow (Drummond and Tahir 1984) is

$$\chi = \frac{a^2}{8\mu_m}\left\{A_0\left[\left(\frac{r}{a}\right)^3 - 2\frac{r}{a} + \frac{a}{r}\right] + C_0\left[\frac{-4r}{a}\ln\left(\frac{r}{a}\right) + \frac{2r}{a} - \frac{2a}{r}\right]\right\}\sin\theta + \frac{a^2}{8\mu_m}\sum_{n=1}^{\infty}\left\{\begin{array}{l} A_n\left[\frac{-1}{n+1}\left(\frac{r}{a}\right)^{2n+3} - \frac{2}{2n+1}\left(\frac{r}{a}\right)^{2n+1} + \frac{1}{(n+1)(2n+1)}\left(\frac{a}{r}\right)^{2n+1}\right] \\ + C_n\left[\frac{-1}{n(2n+1)}\left(\frac{r}{a}\right)^{2n+1} + \frac{1}{n}\left(\frac{a}{r}\right)^{2n-1} - \frac{2}{2n+1}\left(\frac{a}{r}\right)^{2n+1}\right] \end{array}\right\}\sin(2n+1)\theta \quad (33)$$

The velocity profile for flow transverse to adjacent cylinders is then calculated as

$$w_\theta = -\frac{\partial\chi}{\partial r} \quad (34)$$

Using Newton's formula once again, the shear stress acting transverse to the cylinders due to flow is given by

$$\tau^T = \mu_m\frac{\partial w_\theta}{\partial r} \quad (35)$$

Lastly, to estimate the shear stress due to the interaction between the horizontal and vertical struts, the rectangular pores were converted to circular pores using D_{eq}. The extra shear stress on the walls of such pores was calculated as

$$\tau_i^I = \frac{D_{\text{eq}}}{4}\frac{\text{dp}}{\text{d}x_i} \quad (36)$$

3 Methods

The geometry of the vertebral body was idealized to represent that of a rectangular solid with the following physiologically relevant dimensions (Shirazi-Adl et al. 1986):

$l_1 = 48\,\text{mm}$
$l_2 = 33\,\text{mm}$
$l_3 = 21.5\,\text{mm}$

The system of equations derived above was provided with the following initial and constant values:

$E_{\text{T}} = 18\text{GPa}$
$\eta_{\text{T}} = 0.3$
$\phi_0^{\text{f}} = 0.3216$
$\rho_{\text{T}}^{\text{s}} = 1{,}850\ \text{kg/m}^3$
$\rho_{\text{T}}^{\text{m}} = 1{,}250\ \text{kg/m}^3$
$\rho_{\text{T}}^{\text{f}} = 1{,}000\ \text{kg/m}^3$

The controlled input parameters for this model included initial solid volume fraction (ϕ_0^{s}), the primary indicator of bone loss; the amplitude and the frequency of loading, each associated with the vibratory loading stimulus; and the marrow viscosity.

The initial volume fraction of the bone was varied from 0.05 to 0.20 and the amplitude of the vibration, from 1 – 15 $\mu\varepsilon$. In addition, we allowed the frequency to range between 30 and 80 Hz. These frequencies are relevant to laboratory systems used for whole body vibration experiments, but do not include the full range of frequencies observed in bone (Fritton et al. 1997, 2000; Judex et al. 2007), especially during vigorous exercise. Bone loss is associated with elevated fat content in the bone marrow of the vertebral body (Griffith et al. 2005; Yeung et al. 2005), which will affect the rheological properties of the marrow. Herein, we examined the viscosity range 0.1–0.4 Pa s (Bryant et al. 1989). It should be noted, however, that there are few studies that describe the marrow viscosity, an important issue given the fact that its reported value is 100–400 times that of water (0.001 Pa s). The output parameters obtained from the model were interfacial shear stress on the surface of the trabeculae and volumetric flow rate of blood.

4 Results

The shear stress magnitude on each unit cell strut was determined as a function of frequency at ϕ_0^{s} values ranging from 0.05 to 0.20 (Figs. 3, 4). A constant value of 10 $\mu\varepsilon$, representing a mid range level of strain produced by a vibratory loading regimen, was used for this portion of the analysis (Rubin et al. 2002a,b). In addition, we varied apparent strain magnitude, with a constant ϕ_0^{s} of 0.1 (Figs. 5, 6). In general, shear stress on the surface of the trabeculae increased linearly with the frequency of stimulation. While the shear stress on the three struts was the same order of magnitude, the maximum shear was higher on the surface of horizontal struts transverse to the loading direction than on vertical struts. The magnitude of the shear stress was directly related ϕ_0^{s}, the strain magnitude, and the marrow viscosity. In addition, the effect of frequency on shear stress was more pronounced as ϕ_0^{s} increased (Figs. 3, 4). Volume fraction, strain magnitude, and frequency produced similar shear stress magnitudes over the respective range of values used for this study, but marrow viscosity proved the most influential factor in determining peak shear stress magnitude (Figs. 3, 4, 5 6).

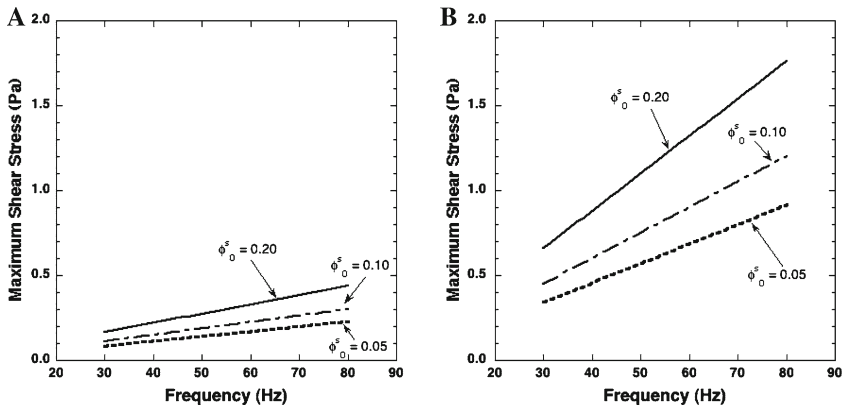

Fig. 3 The maximum shear stress magnitude on a vertical strut as a function of frequency and ϕ_0^s values ranging from 0.05 to 0.20. A constant value of 10 microstrain was used as the amplitude of vibration for this portion of the analysis and the effect of viscosity was examined by using $\mu_m = 0.1$ Pa s **a** or $\mu_m = 0.4$ Pa s **b** With increasing viscosity, the shear stress increases as does its sensitivity to frequency and ϕ_0^s

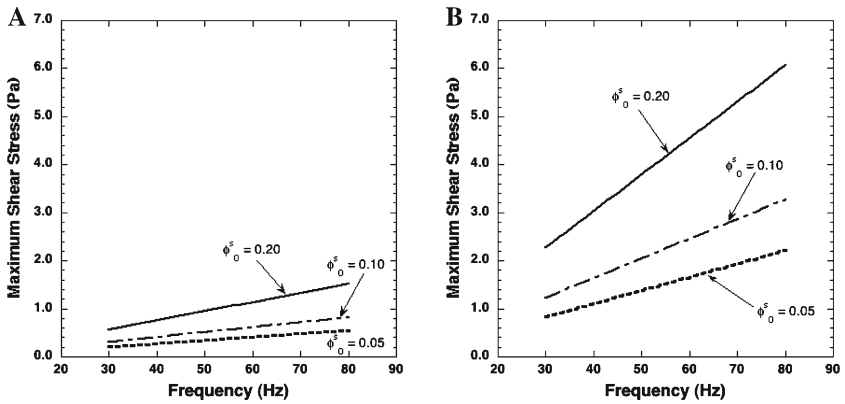

Fig. 4 The maximum shear stress magnitude on the horizontal strut lying along the 1-axis as a function of frequency and ϕ_0^s values ranging from 0.05 to 0.20. A constant value of 10 microstrain was used as the amplitude of vibration for this portion of the analysis and the effect of viscosity was examined by using $\mu_m = 0.1$ Pa s **a** or $\mu_m = 0.4$ Pa s **b** The magnitude of the shear stress on the horizontal strut is substantially greater than that exerted on the vertical struts. With increasing viscosity, the shear stress increases as does its sensitivity to frequency and ϕ_0^s

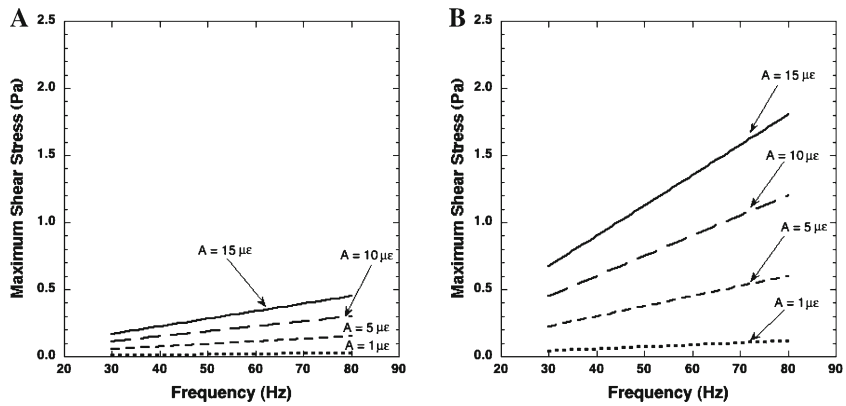

Fig. 5 Maximum shear stress on the vertical strut as a function of frequency and the amplitude of apparent strain. A constant value of 0.1 was used for ϕ_0^s. Shear stress magnitude increases with increasing frequency and with increasing apparent strain. The effect of viscosity was examined by using $\mu_m = 0.1$ Pa s **a** or $\mu_m = 0.4$ Pa s **b** Increasing the viscosity increased the maximum shear stress as well as the sensitivity to the magnitude of the vibration

The boundaries of the vertebral body in this model require that all volume loss during deformation be attributed to blood exiting the trabecular framework. The peak volumetric flow rate of blood was predicted as a function of ϕ_0^s, macroscopic strain level, and frequency as primary input parameters, in an analysis similar to that performed above for the shear stress and ranged from 0.1 to 0.35 ml/s. Flow rate increased linearly both with increasing vibrational frequency and with decreasing ϕ_0^s (Figs. 7, 8). Interestingly, there was only a 6.3% difference in blood flow rate even at the highest frequency (80 Hz) between the extreme input values of ϕ_0^s. In contrast, increasing the macroscopic strain magnitude from 1 to 15 $\mu\varepsilon$ substantially increased the blood flow rate (Fig. 8).

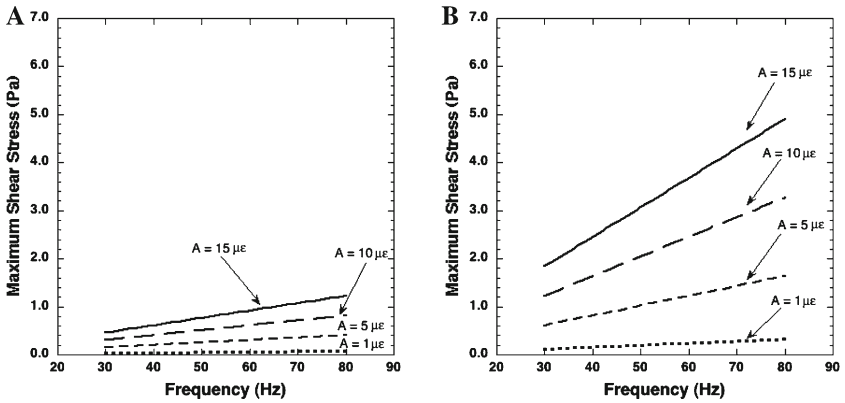

Fig. 6 Maximum shear stress on the horizontal strut along the 1-axis as a function of frequency and the amplitude of apparent strain. A constant value of 0.1 was used for ϕ_0^s. Shear stress magnitude increases with increasing frequency and with increasing apparent strain. The effect of viscosity was examined by using $\mu_m = 0.1$ Pa s **a** or $\mu_m = 0.4$ Pa s **b** Increasing the viscosity increased the maximum shear stress as well as the sensitivity to the magnitude of the vibration. Similar results also observed for the strut along the 2-axis

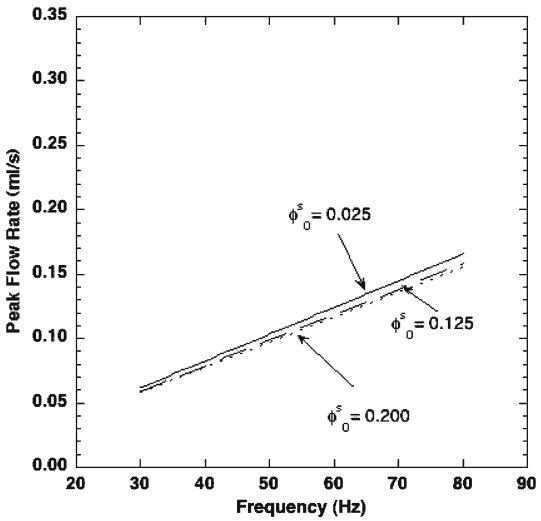

Fig. 7 Peak blood flow rate as a function of frequency and ϕ_0^s. Holding the apparent strain constant at 10 microstrain yielded a linear increase in peak blood flow rate as frequency increased. The flow rate increased slightly as ϕ_0^s increased with less than a 10% difference between the highest and lowest ϕ_0^s at any given frequency

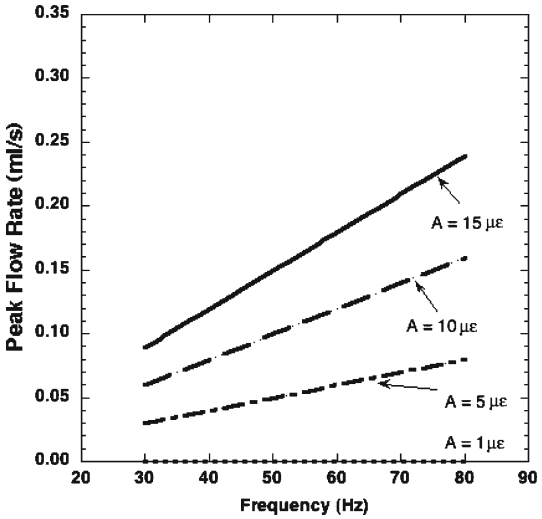

Fig. 8 Peak blood flow rate as a function of frequency and apparent strain. A constant value of 0.1 was used for ϕ_0^s. There was a linear increase in peak blood flow rate as frequency increased. The flow rate increased as the apparent strain amplitude increased. The peak flow rate was more sensitive to frequency at higher apparent strain magnitudes

5 Discussion

In this study, a mixture theory model of the vertebral body complemented by a cellular solid representation of the cancellous bone was employed to explore the mechanical consequences of vibratory loading by perturbations in input parameters. The effects of apparent strain magnitude, frequency, and porosity on two of the deformation-induced output parameters (interfacial shear stress and volumetric blood flow rate) were determined. One of this study's primary findings was that the maximum shear stresses on the surfaces of the trabeculae during vibratory loading reach magnitudes on the order of what has been found to be stimulatory for osteoblasts in vitro (Klein-Nulend et al. 1995a,b; Nauman et al. 2001; Kapur et al. 2003). Over the range of frequencies typically used for in vivo vibration studies (30–50 Hz), the peak interfacial shear stresses on model trabeculae ranged from 0.1–2.0 Pa (1–20 dynes/cm^2) at an amplitude of 10 μm. In all cases, increasing frequency produced an increase in the shear stress. Increasing the amplitude of the vibration also yielded a proportional increase in shear stress. Interestingly, the larger strain amplitudes produced a more pronounced change in the shear stress magnitude with frequency at a mid-range initial solid volume fraction. It should be noted, however, that marrow viscosity was the single most important factor in determining the fluid shear stress acting on the surfaces of the trabeculae. Bone loss and increased bone marrow fat content are well correlated (Griffith et al. 2005; Yeung et al. 2005), and such a change in the

composition of bone marrow will alter the viscosity. In this model, an increase in marrow viscosity was shown to increase shear stress proportionally. In osteoporotic individuals, this could mean that vibration would introduce peak shear stresses to a magnitude that is experienced by healthy individuals. Unfortunately, the rheological properties of the marrow are not very well characterized. To the authors' knowledge, Bryant et al. (1989) have performed the only study to date to experimentally determine such properties. Further studies to determine marrow properties and correlate them with changes in composition are needed.

Peak volumetric blood flow rates of the order of 0.1–0.35 ml/s were predicted by the model. As seen with shear stress, variations in strain amplitude with a constant initial solid volume fraction produced proportional increases in the volumetric flow rate. Volumetric flow rate was also more sensitive to frequency at higher strain magnitudes. Varying the initial solid volume fraction, however, produced a different response than that seen with shear stress. Although the peak volumetric flow rate did increase as the solid volume fraction was decreased, the increase was marginal. Viewing peak blood flow rate as a measure of transport, this result suggests that increased nutrient transport is a contributing mechanism to the difference in anabolic response between normal and osteoporotic bone subjected to a vibratory stimulus.

These results have some implications for the bone adaptation observed in response to application of the whole body vibration. There are a number of possible explanations for the experimental observation that whole body vibration is anabolic to bone, especially in the cancellous bone of postmenopausal women and children with low bone mineral density (Rubin et al. 2004; Verschueren et al. 2004; Ward et al. 2004; Iwamoto et al. 2005). The deformation and its byproducts, including intramedullary pressure, transport due to fluid flow, and fluid shear stress, have been listed as possible causal mechanisms for the observed response. In addition, it has been theorized that osteoporosis results from a symptomatic loss of muscular contraction adjacent to the bone that produces regularly occurring high frequency, low strain mechanical stimuli (Huang et al. 1999). Whole body vibration may reintroduce a component of these signals, while healthy individuals would experience no substantial deviations from the normal local mechanical environment.

To date, however, we are not aware of any studies that have explored the specific mechanical stimuli by which such low level signals are able to promote bone formation in cancellous bone. In a sheep model, Rubin et al. (2002a,b) observed increases in cancellous bone quantity and quality following vibratory loading with no effect on cortical bone. These animal studies provided the impetus for several human trials with vibratory loading. While the loading was not found to be effective in increasing the bone mass of young, healthy human subjects (Torvinen et al. 2003), in osteoporotic patients, whole body vibration was able to either abate bone loss or stimulate increases in bone mass (Rubin et al. 2004; Verschueren et al. 2004). Interestingly, Xie et al. (2006) found that whole body vibration caused a decrease in osteoclastic resorption on the trabeculae, suggesting that one or more signals act to inhibit the catabolic response. Along with the signal provided by the strain itself, deformation-induced events, particularly fluid flow, have been implicated in bone remodeling. Oscillatory fluid flow within the structure induces shear stress on the surface of the trabeculae and additional chemotransport due to blood flow. Combining the predicted effects of volume fraction on fluid shear stress and blood transport with experimental observations that note better osteogenic response in less dense bone, suggests that shear stress may be the most important physiological cue for anabolic activity in cancellous bone under vibratory loading. If so, the response of osteoclasts to fluid shear stresses, may be an appropriate area of future research (Xie et al. 2006). In addition, this model suggests that vibrations in the vertical direction will lead to increased bone formation on the horizontal struts where the peak shear stresses were observed. If the aim is to increase compressive stiffness, it may be more appropriate to apply the vibratory loading in the transverse direction. In order to test this hypothesis, one would need to perform experiments wherein measurements were made of new bone formation (Judex et al. 2007) while accounting for the orientation of each trabeculae. Recent work by (Judex et al. 2007) indicated that low magnitude vibratory signals ($\sim$1 $\mu\varepsilon$) at 45 Hz did not stimulate bone formation in the rat proximal tibia while lower amplitude signals ($\sim$0.4 $\mu\varepsilon$) at 90 Hz were anabolic. While these differences indirectly support the notion that fluid shear stress is the stimulatory signal, no definitive conclusions can be drawn until the differences in geometry have been taken into account. In contrast, fluid transport appears to be much more important to the adaptive response in cortical bone (Knothe Tate et al. 2000; Knothe Tate 2003), where the dense structure makes it difficult to transport nutrients and oxygen to the osteocytes and osteoblasts housed therein.

This mixture theory-based model provides a closed-form solution for the fluid shear stress and volumetric blood flow rate using only the magnitude of the applied vibratory load as an input parameter. Model parameters can be easily changed to determine the sensitivity of the model to a variety of physiological factors and it begins to elucidate experimentally observed phenomena. As such, the model is a simplification of the complex interaction of several tissue components. It should be noted that we examined a range of models including two phase (bone and marrow), the three phase (bone, marrow, and blood) model described herein, and a five phase (bone, marrow, artery space, vein space, and capillary bed). Of these possible descriptions, the three phase model provided enough complexity to yield reasonable mechanical

results while requiring only a few, easily obtained boundary conditions. Because three phases were needed for the mathematical description, this technique required mixture theory and did not offer the opportunity for comparison to simpler two phase models such as those developed by Biot and coworkers (Biot 1941; Rice and Cleary 1976).

Potential limitations of the study include inaccuracies resulting from the simplified geometry of the cancellous bone used to predict material properties, the difficulty in determining material parameters such as marrow viscosity and blood volume fraction for a given individual, and the assumption of marrow as a Newtonian fluid. While the simplified cancellous bone geometry is a limitation, compared with other anatomic sites, the vertebral body has a relatively uniform geometry. In addition, the model was calibrated to experimental data (Kopperdahl and Keaveny 1998; Sander et al. 2003) over a large range of volume fractions. The viscoelastic response of the trabecular tissue may influence the deformation of the cancellous bone at high strain rates, but for the small strains considered here the effects should be minimal even at higher frequencies. Material parameters such as marrow viscosity and blood volume fraction are difficult to determine for individual patients, but some information, such as fat content of the marrow can be determined from magnetic resonance imaging (Vande Berg et al. 1998; Griffith et al. 2005). High fat content in the marrow has been linked to increased bone remodeling (Martin et al. 1990) and this may be related to the increased marrow viscosity. Future work is needed to characterize the relationship between marrow viscosity and fat content as well as other patient parameters such as age and body mass index. Future work in this area is especially important given the fact that published reports of marrow viscosity indicate that it is 100–400 times more viscous than water, thus accounting for the relatively high shear stresses obtained in this study. Initial blood volume fraction likely varies considerably between patients, but appears to be less important than fluid shear stress for determining the osteogenic response in vertebral cancellous bone. Finally, the assumption that the marrow behaves as a Newtonian fluid is a fruitful starting point, but requires experimental verification. Ex vivo experiments by Bryant suggests that marrow can be approximated as a Newtonian fluid, but new techniques must be developed to estimate marrow viscosity in situ, something that has not been accomplished to date. Such experiments will likely find that the rheology of bone marrow requires advanced continuum models for accurate representation.

While the model is based on an idealized geometry, it provides a basis for further experimental studies. In the future, this model could be combined with additional mechanical models of the spine as a vibrating system (Fritz 2000; Guo and Teo 2005; Makhsous et al. 2005) in order to better understand the relationship between vibration amplitude and frequency as these parameters will depend on interpatient differences in height, weight, vertebrae size and structure. From a biological perspective, this model could be used in conjunction with studies on the genetic basis of osteoporosis. Genetic differences have been linked to variations in bone size, bone quality, and remodeling rates (Huang and Kung 2006; Liu et al. 2006) as well as the biophysical response of bone cells to fluid shear stress (Burger et al. 1995; Klein-Nulend et al. 1995a,b).

In conclusion, this mixture theory-based model predicts shear stresses on the surfaces of the trabeculae and volumetric blood flow rates as functions of the applied whole-body vibrations. Further experiments are needed to verify and extend the results of this model. In particular, animal models which measure the blood flow into and out of the vertebral body can be used to better calibrate the model. Taken together, these data will provide a basis for determining which patients will best respond to whole body vibration and further elucidate the mechanotransduction pathways for bone cells in vivo.

Acknowledgments The authors would like to thank the Whitaker Foundation and the National Science Foundation for financial support in the form of graduate fellowships. We would also like to thank Daniel Shimko for rendering Fig. 2 and David Van Sickle and Alan Burshell for many helpful discussions. In addition, the administrative support provided by Michelle Sarault was instrumental in the completion of this study.

References

Abbott TA, Lawrence BJ, Wallach S (1996) Osteoporosis: the need for comprehensive treatment guidelines. Clin Ther 18(1):127–149; discussion 126

Atkin R, Craine R (1976a) Continuum Theory of Mixtures: Applications. J Institute Math Appl 17(2):153–207

Atkin R, Craine R (1976b) Continuum theory of mixtures: basic theory and historical development. Q J Mech Appl Math 29:209–244

Biot MA (1941) General theory of three-dimensional consolidation. J Appl Phys 12:155–164

Bryant JD, David T, Gaskell PH, King S, Lond G (1989) Rheology of bovine bone marrow. Proc Inst Mech Eng [H] 203(2):71–75

Burger EH, Klein-Nulend J, van der Plas A, Nijweide PJ (1995) Function of osteocytes in bone–their role in mechanotransduction. J Nutr 125(7 Suppl):2020S–2023S

Cowin SC, Weinbaum S, Zeng Y (1995) A case for bone canaliculi as the anatomical site of strain generated potentials. J Biomech 28(11):1281–1297

Currey J (1984) The mechanical adaptations of bones. Princeton, Princeton University Press

Davidson MR (2003) Pharmacotherapeutics for osteoporosis prevention and treatment. J Midwifery Womens Health 48(1):39–52

Drummond J, Tahir M (1984) Laminar Viscous-Flow Through Regular Arrays of Parallel Solid Cylinders. Int J Multiphase Flow 10(5):515–540

Flieger J, Karachalios T, Khaldi L, Raptou P, Lyritis G (1998) Mechanical stimulation in the form of vibration prevents postmenopausal bone loss in ovariectomized rats. Calcif Tissue Int 63(6):510–514

Fourie JG, Du Plessis JP (2002) Pressure drop modeling in cellular metallic foams. Chem Eng Sci 57:2781–2789

Fritton JC, Rubin CT, Qin YX, McLeod KJ (1997) Whole-body vibration in the skeleton: development of a resonance-based testing device. Ann Biomed Eng 25(5):831–839

Fritton SP, McLeod KJ, Rubin CT (2000) Quantifying the strain history of bone: spatial uniformity and self-similarity of low-magnitude strains. J Biomech 33(3):317–325

Fritz M (2000) Simulating the response of a standing operator to vibration stress by means of a biomechanical model. J Biomech 33(7):795–802

Griffith JF, Yeung DK, Antonio GE, Lee FK, Hong AW, Wong SY, Lau EM, Leung PC (2005) Vertebral bone mineral density, marrow perfusion, and fat content in healthy men and men with osteoporosis: dynamic contrast-enhanced MR imaging and MR spectroscopy. Radiology 236(3):945–951

Guo LX, Teo EC (2005) Prediction of the modal characteristics of the human spine at resonant frequency using finite element models. Proc Inst Mech Eng [H] 219(4):277–284

Huang QY, Kung AW (2006) Genetics of osteoporosis. Mol Genet Metab 88(4):295–306

Huang RP, Rubin CT, McLeod KJ (1999) Changes in postural muscle dynamics as a function of age. J Gerontol A Biol Sci Med Sci 54(8):B352–B357

Iwamoto J, Takeda T, Sato Y, Uzawa M (2005) Effect of whole-body vibration exercise on lumbar bone mineral density, bone turnover, and chronic back pain in post-menopausal osteoporotic women treated with alendronate. Aging Clin Exp Res 17(2):157–163

Judex S, Donahue LR, Rubin C (2002) Genetic predisposition to low bone mass is paralleled by an enhanced sensitivity to signals anabolic to the skeleton. Faseb J 16(10):1280–1282

Judex S, Boyd S, Qin YX, Turner S, Ye K, Muller R, Rubin C (2003) Adaptations of trabecular bone to low magnitude vibrations result in more uniform stress and strain under load. Ann Biomed Eng 31(1):12–20

Judex S, Lei X, Han D, Rubin C (2007) Low-magnitude mechanical signals that stimulate bone formation in the ovariectomized rat are dependent on the applied frequency but not on the strain magnitude. J Biomech 40(6):1333–1339

Kapur S, Baylink DJ, Lau KH (2003) Fluid flow shear stress stimulates human osteoblast proliferation and differentiation through multiple interacting and competing signal transduction pathways. Bone 32(3):241–251

Keaveny TM, Morgan EF, Niebur GL, Yeh OC (2001) Biomechanics of trabecular bone. Annu Rev Biomed Eng 3:307–333

Klein-Nulend J, van der Plas A, Semeins CM, Ajubi NE, Frangos JA, Nijweide PJ, Burger EH (1995a) Sensitivity of osteocytes to biomechanical stress in vitro. Faseb J 9(5):441–445

Klein-Nulend J, van der Plas A, Semeins CM, Ajubi NE, Frangos JA, Nijweide PJ, Burger EH (1995b) Sensitivity of osteocytes to biomechanical stress in vitro. Faseb J 9(5):441–445

Knothe Tate ML (2003) Whither flows the fluid in bone? An osteocyte's perspective. J Biomech 36(10):1409–1424

Knothe Tate ML, Steck R, Forwood MR, Niederer P (2000) In vivo demonstration of load-induced fluid flow in the rat tibia and its potential implications for processes associated with functional adaptation. J Exp Biol 203(Pt 18):2737–2745

Kopperdahl DL, Keaveny TM (1998) Yield strain behavior of trabecular bone. J Biomech 31(7):601–608

Liu YJ, Shen H, Xiao P, Xiong DH, Li LH, Recker RR, Deng HW (2006) Molecular genetic studies of gene identification for osteoporosis: a 2004 update. J Bone Miner Res 21(10):1511–1535

Makhsous M, Hendrix R, Crowther Z, Nam E, Lin F (2005) Reducing whole-body vibration and musculoskeletal injury with a new car seat design. Ergonomics 48(9):1183–1199

Martin RB, Chow BD, Lucas PA (1990) Bone marrow fat content in relation to bone remodeling and serum chemistry in intact and ovariectomized dogs. Calcif Tissue Int 46(3):189–194

Morgan EF, Keaveny TM (2001) Dependence of yield strain of human trabecular bone on anatomic site. J Biomech 34(5):569–577

Morgan EF, Yeh OC, Chang WC, Keaveny TM (2001) Nonlinear behavior of trabecular bone at small strains. J Biomech Eng 123(1): 1–9

Mosekilde L (1988) Age-related changes in vertebral trabecular bone architecture–assessed by a new method. Bone 9(4):247–250

Nauman EA, Satcher RL, Keaveny TM, Halloran BP, Bikle DD (2001) Osteoblasts respond to pulsatile fluid flow with short-term increases in PGE(2) but no change in mineralization. J Appl Physiol 90(5):1849–1854

Otter MW, Palmieri vR, Cochran GVB (1990) Transcortical Streaming Potentials are Generated by Circulatory Pressure Gradients in Living Canine Tibia. J Orthop Res 8:119–126

Owan I, Burr DB, Turner CH, Qiu J, Tu Y, Onyia JE, Duncan RL (1997) Mechanotransduction in bone: osteoblasts are more responsive to fluid forces than mechanical strain. Am J Physiol 273(3 Pt 1):C810–C815

Piekarski K, Munro M (1977) Transport mechanism operating between blood supply and osteocytes in long bones. Nature 269(5623):80–82

Rice JR, Cleary MP (1976) Some basic diffusion solutions for fluid-saturated elastic porous media with compressible constituents. Rev Geophys Space Phys 14(2):227–241

Roelofsen J, Kleinnulend J, Burger EH (1995) Mechanical Stimulation By Intermittent Hydrostatic Compression Promotes Bone-Specific Gene Expression In Vitro. J Biomech 28(12):1493–1503

Routh RH, Rumancik S, Pathak RD, Burshell AL, Nauman EA (2005) The relationship between bone mineral density and biomechanics in patients with osteoporosis and scoliosis. Osteoporos Int 16(12):1857–1863

Rubin C, Turner AS, Bain S, Mallinckrodt C, McLeod K (2001) Anabolism. Low mechanical signals strengthen long bones. Nature 412(6847):603–604

Rubin C, Turner AS, Mallinckrodt C, Jerome C, McLeod K, Bain S (2002a) Mechanical strain, induced noninvasively in the high-frequency domain, is anabolic to cancellous bone, but not cortical bone. Bone 30(3):445–452

Rubin C, Turner AS, Muller R, Mittra E, McLeod K, Lin W, Qin YX (2002b) Quantity and quality of trabecular bone in the femur are enhanced by a strongly anabolic, noninvasive mechanical intervention. J Bone Miner Res 17(2):349–357

Rubin C, Recker R, Cullen D, Ryaby J, McCabe J, McLeod K (2004) Prevention of postmenopausal bone loss by a low-magnitude, high-frequency mechanical stimuli: a clinical trial assessing compliance, efficacy, and safety. J Bone Miner Res 19(3):343–351

Rumancik S, Routh RH, Pathak RD, Burshell AL, Nauman EA (2005) Assessment of bone quantity and distribution in adult lumbar scoliosis: new dual-energy x-ray absorptiometry methodology and analysis. Spine 30(4):434–439

Sander EA, Shimko DA, Dee KC, Nauman EA (2003) Examination of continuum and micro-structural properties of human vertebral cancellous bone using combined cellular solid models. Biomech Model Mechanobiol 2(2):97–107

Shirazi-Adl A, Ahmed AM, Shrivastava SC (1986) A finite element study of a lumbar motion segment subjected to pure sagittal plane moments. J Biomech 19(4):331

Torvinen S, Kannus P, Sievanen H, Jarvinen TA, Pasanen M, Kontulainen S, Nenonen A, Jarvinen TL, Paakkala T, Jarvinen M, Vuori I (2003) Effect of 8-month vertical whole body vibration on bone, muscle performance, and body balance: a randomized controlled study. J Bone Miner Res 18(5):876–884

Turner CH, Pavalko FM (1998) Mechanotransduction and functional response of the skeleton to physical stress: the mechanisms and mechanics of bone adaptation. Journal of Orthopaedic Sci 3(6):346–355

Vande Berg BC, Malghem J, Lecouvet FE, Maldague B (1998) Magnetic resonance imaging of normal bone marrow. Eur Radiol 8(8): 1327–1334

Verschueren SM, Roelants M, Delecluse C, Swinnen S, Vanderschueren D, Boonen S (2004) Effect of 6-month whole body vibration training on hip density, muscle strength, and postural control in postmenopausal women: a randomized controlled pilot study. J Bone Miner Res 19(3):352–359

Ward K, Alsop C, Caulton J, Rubin C, Adams J, Mughal Z (2004) Low magnitude mechanical loading is osteogenic in children with disabling conditions. J Bone Miner Res 19(3):360–369

Weinbaum S, Cowin SC, Zeng Y (1994) A model for the excitation of osteocytes by mechanical loading-induced bone fluid shear stresses. J Biomech 27(3):339–360

Xie L, Jacobson JM, Choi ES, Busa B, Donahue LR, Miller LM, Rubin CT, Judex S (2006) Low-level mechanical vibrations can influence bone resorption and bone formation in the growing skeleton. Bone 39(5):1059–1066

Yeung DK, Griffith JF, Antonio GE, Lee FK, Woo J, Leung PC (2005) Osteoporosis is associated with increased marrow fat content and decreased marrow fat unsaturation: a proton MR spectroscopy study. J Magn Reson Imaging 22(2):279–285